

1

Basic Principles of Fluorescence Spectroscopy

1.1

Absorption and Emission of Light

As fluorophores play the central role in fluorescence spectroscopy and imaging we will start with an investigation of their manifold interactions with light. A fluorophore is a component that causes a molecule to absorb energy of a specific wavelength and then re-emit energy at a different but equally specific wavelength. The amount and wavelength of the emitted energy depend on both the fluorophore and the chemical environment of the fluorophore. Fluorophores are also denoted as chromophores, historically speaking the part or moiety of a molecule responsible for its color. In addition, the denotation chromophore implies that the molecule absorbs light while fluorophore means that the molecule, likewise, emits light. The umbrella term used in light emission is luminescence, whereas fluorescence denotes allowed transitions with a lifetime in the nanosecond range from higher to lower excited singlet states of molecules.

In the following we will try to understand why some compounds are colored and others are not. Therefore, we will take a closer look at the relationship of conjugation to color with fluorescence emission, and investigate the absorption of light at different wavelengths in and near the visible part of the spectrum of various compounds. For example, organic compounds (i.e., hydrocarbons and derivatives) without double or triple bonds absorb light at wavelengths below 160 nm, corresponding to a photon energy of $>180 \text{ kcal mol}^{-1}$ ($1 \text{ cal} = 4.184 \text{ J}$), or $>7.8 \text{ eV}$ (Figure 1.1), that is, significantly higher than the dissociation energy of common carbon-to-carbon single bonds.

Below a wavelength of 200 nm the energy of a single photon is sufficient to ionize molecules. Therefore, photochemical decomposition is most likely to occur when unsaturated compounds, where all bonds are formed by σ -electrons, are irradiated with photon energies $>6.2 \text{ eV}$. Double and triple bonds also use π -electrons in addition to a σ -bond for bonding. In contrast to σ -electrons, which are characterized by the rotational symmetry of their wavefunction with respect to the bond direction, π -electrons are characterized by a wavefunction having a node at the nucleus and rotational symmetry along a line through the nucleus. π -bonds

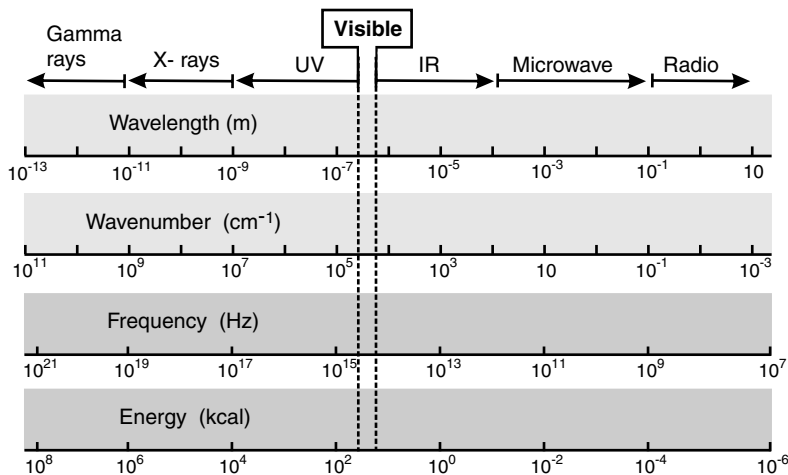


Figure 1.1 The electromagnetic spectrum.

are usually weaker than σ -bonds because their (negatively charged) electron density is further from the positive charge of the nucleus, which requires more energy. From the perspective of quantum mechanics, this bond weakness is explained by significantly less overlap between the component π -orbitals due to their parallel orientation. These less strongly bound electrons can be excited by photons with lower energy. If two double bonds are separated by a single bond, the double bonds are termed conjugated. Conjugation of double bonds further induces a red-shift in the absorption (a so-called bathochromic shift). All fluorophores that have a high absorption in the visible part of the spectrum possess several conjugated double bonds.

Above 200 nm only the two lowest energy transitions, that is, $n \rightarrow \pi^*$ and $\pi \rightarrow \pi^*$, are achieved as a result of the energy available from the photons. When sample molecules are exposed to light having an energy that matches a possible electronic transition within the molecule, some of the light energy will be absorbed as the electron is promoted to a higher energy orbital. As a simple rule, energetically favored electron promotion will be from the highest occupied molecular orbital (HOMO), usually the singlet ground state, S_0 , to the lowest unoccupied molecular orbital (LUMO), and the resulting species is called the singlet excited state S_1 . Absorption bands in the visible region of the spectrum correspond to transitions from the ground state of a molecule to an excited state that is $40\text{--}80 \text{ kcal mol}^{-1}$ above the ground state. As mentioned previously, in saturated hydrocarbons in particular, the lowest electronic states are more than 80 kcal mol^{-1} above the ground state, and therefore they do not absorb light in the visible region of spectrum. Such substances are not colored. Compounds that absorb in the visible region of the spectrum (these compounds have color) generally have some weakly bound or delocalized electrons. In these systems, the energy difference between the lowest LUMO and the HOMO corresponds to the energies of quanta in the visible region.

On the other side of the electromagnetic spectrum, there is a natural limit to long-wavelength absorption and emission of fluorophores, which is in the region of $1\text{ }\mu\text{m}$ [1]. A dye absorbing in the near-infrared ($>700\text{ nm}$) has a low-lying excited singlet state and even slightly lower than that, a metastable triplet state, that is, a state with two unpaired electrons that exhibits biradical character. Even though no generally valid rule can be formulated predicting the thermal and photochemical stability of fluorophores, the occupation of low-lying excited singlet and triplet states potentially increases the reactivity of fluorophores. Therefore, it is likely that fluorophores with long-wavelength absorption and emission will show less thermal and photochemical stability, due to reactions with solvent molecules such as dissolved oxygen, impurities, and other fluorophores. In addition, with increasing absorption, that is, with a decreasing energy difference between S_1 and S_0 , the fluorescence intensity of fluorophores decreases owing to increased internal conversion. That is, with a decreasing energy difference between the excited and ground state, the number of options to get rid of the excited-state energy by radiationless deactivation increases. Hence, most known stable and bright fluorophores absorb and emit in the wavelength range between 300 and 700 nm.

Fluorophores with conjugated doubled bonds (polymethine dyes) are essentially planar, with all atoms of the conjugated chain lying in a common plane linked by σ -bonds. π -electrons, on the other hand, have a node in the plane of the molecule and form a charge cloud above and below this plane along the conjugated chain (Figure 1.2). The visible bands for polymethine dyes arise from electronic transitions involving the π -electrons along the polymethine chain. The wavelength of these bands depends on the spacing of the electronic levels. The absorption of light by fluorophores such as polymethine dyes can be understood semiquantitatively by applying the free-electron model proposed by Kuhn [2, 3]. The arrangement of alternating single–double bonds in an organic molecule usually implies that the π -electrons are delocalized over the framework of the “conjugated” system. As these π -electrons are mobile throughout the carbon atom skeleton containing the alternating double bonds, a very simple theoretical model can be applied to such a system in order to account for the energy of these electrons in the molecule. If one makes the

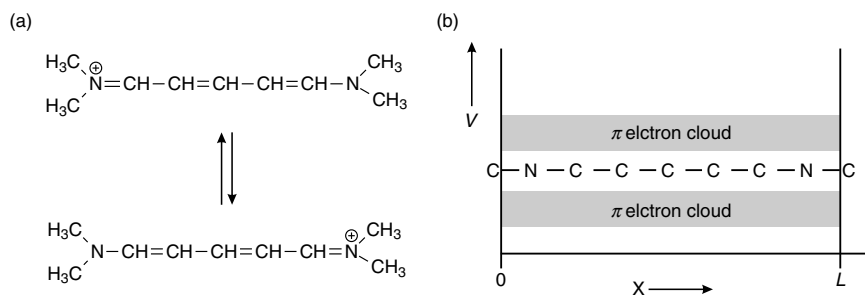


Figure 1.2 (a) Limiting structures of a resonance hybrid of a simple positively charged cyanine dye. (b) The π -electron cloud of the cyanine dye as seen from the side in a simplified potential energy (V) trough of length L .

seemingly drastic assumption that the several π -electrons that comprise the system are non-interacting (presumably, if the π -electrons are delocalized over the $-\text{C}=\text{C}-\text{C}=\text{C}-\text{C}=\text{C}-$ framework, they spread out, minimizing repulsion between them), then one can view the energetics of this system as arising from the simple quantum mechanical assembly of one-electron energy levels appropriate to the *particle in the box model*. In this case, one considers the potential energy of the electron as being constant throughout the length of the molecular box and then rising to infinity at each end of the conjugated portion of the molecule. As an example, consider a positively charged simple cyanine dye. The cation can “resonate” between the two limiting structures shown in Figure 1.2a, that is, the wavefunction for the ion has equal contributions from both states. Thus, all the bonds along this chain can be considered equivalent, with a bond order of 1.5, similar to the C–C bonds in benzene.

Assuming that the conjugated chain extends approximately one bond length to the left and right beyond the terminal nitrogen atoms, application of the Schrodinger equation to this problem results in the well known expressions for the wavefunctions and energies, namely:

$$\psi_n = \sqrt{\frac{2}{L}} \sin\left(\frac{n\pi x}{L}\right)$$

and

$$E_n = \frac{n^2 h^2}{8 mL^2}$$

where

n is the quantum number ($n = 1, 2, 3, \dots$) giving the number of antinodes of the eigenfunction along the chain

L is the “length” of the (one dimensional) molecular box

m is the mass of the particle (electron)

h is Planck’s constant

x is the spatial variable, which is the displacement along the molecular backbone.

Each wavefunction can be referred to as a molecular orbital, and its respective energy is the orbital energy. If the spin properties of the electron are taken into account along with the *ad hoc* invocation of Pauli’s exclusion principle, the model is then refined to include spin quantum numbers for the electron ($1/2$) along with the restriction that no more than two electrons can occupy a given wavefunction or level, and the spin quantum numbers of the two electrons occupying a given energy level are opposite (spin up and spin down). Thus, if we have N electrons, the lower states are filled with two electrons each, while all higher states are empty provided that N is an even number (which is usually the case in stable molecules as only highly reactive radicals possess an unpaired electron). This allows the electronic structure for the π -electrons in a conjugated dye molecule to be constructed. For example, for the conjugated molecule $\text{CH}_2=\text{CH}-\text{CH}=\text{CH}-\text{CH}=\text{CH}_2$ 6 π -electrons have to be considered. The lowest energy configuration, termed the electronic ground state,

corresponds to the six electrons being in the lowest three orbitals. Higher energy configurations are constructed by promoting an electron from the HOMO with quantum number $n = 3$ to the LUMO with $n = 4$. This higher energy arrangement is called the electronically excited singlet state. The longest wavelength absorption band corresponds to the energy difference between these two states, which is then given by the following expression:

$$\Delta E = E_{\text{LUMO}} - E_{\text{HOMO}} = \frac{h^2}{8mL^2} (n_{\text{LUMO}}^2 - n_{\text{HOMO}}^2)$$

The energy required for this electronic transition can be supplied by a photon of the appropriate frequency, given by the Planck relationship:

$$E = h\nu = hc/\lambda$$

where

h is Planck's constant

ν is the frequency

c is the speed of light

λ is the wavelength.

Because the ground state of a molecule with N π -electrons will have $N/2$ lowest levels filled and all higher levels empty, we can write $n_{\text{LUMO}} = N/2 + 1$ and $n_{\text{HOMO}} = N/2$:

$$\Delta E = \frac{h^2}{8mL^2} (N+1) \quad \text{or} \quad \lambda = \frac{8mc}{h} \frac{L^2}{N+1}$$

This indicates that to a first approximation the position of the absorption band is determined only by the chain length and the number of delocalized π -electrons. Good examples for this relationship are symmetrical cyanine dyes of the general formula shown in Figure 1.2a.

1.2

Spectroscopic Transition Strengths

The probability of a molecule changing its state by absorption or emission of a photon depends on the nature of the wavefunctions of the initial and final states, how strongly light can interact with them, and on the intensity of any incident light. The probability of a transition occurring is commonly described by the transition strength. To a first approximation, transition strengths are governed by selection rules that determine whether a transition is allowed or disallowed. In the classical theory of light absorption, matter consists of an array of charges that can be set into motion by the oscillating electromagnetic field of the light. Here, the electric dipole oscillators set in motion by the light field have specific natural characteristics, that is, frequencies, ν_i , that depend on the material. When the frequency of the radiation is near the oscillator frequency, absorption occurs, and the intensity of the radiation

decreases on passing through the substance. The intensity of the interaction is known as the oscillator strength, f_i , and it can be thought of as characterizing the number of electrons per molecule that oscillate with the characteristic frequency, ν_i . Therefore, practical measurements of the transition strength are usually described in terms of f_i . The oscillator strength of a transition is a dimensionless number that is useful for comparing different transitions. For example, a transition that is fully allowed quantum mechanically is said to have an oscillator strength of 1.0. Experimentally, the oscillator strength, f , is related to the intensity of absorption, that is, to the area under an absorption band plotted versus the frequency.

$$f = \frac{2303}{\pi N_A} \frac{mc}{e^2 n} \int \epsilon(\nu) d\nu$$

where

ϵ is the molar absorptivity

c is the velocity of light

m is the mass of an electron

e is the electron charge

n is the refractive index of the medium,

N_A is Avogadro's number.

The integration is carried out over the frequency range associated with the absorption band.

The quantum mechanical description, which is the most satisfactory and complete description of the absorption of radiation by matter, is based on time-dependent wave mechanics. Here, a transition from one state to another occurs when the radiation field connects the two states. In wave mechanics, the connection is described by the transition dipole moment, μ_{GE} :

$$\mu_{GE} = \int \psi_G \mu \psi_E dv$$

where

ψ_G and ψ_E are the wavefunctions for the ground and excited state, respectively
 dv represents the volume element.

The transition dipole moment will be nonzero whenever the symmetry of the ground and excited states differ. For example, ethylene ($\text{CH}_2=\text{CH}_2$) has no permanent dipole moment, but if ψ_G is a π -molecular orbital and ψ_E is a π^* -molecular orbital, then $\mu_{\pi\pi^*}$ is not zero. The direction of the transition moment is characterized by the vector components: $\langle \mu_x \rangle_{GE}$, $\langle \mu_y \rangle_{GE}$, and $\langle \mu_z \rangle_{GE}$. It has to be pointed out that for most transitions the three vectors are not all equal, that is, the electronic transition is polarized. The ethylene $\pi \rightarrow \pi^*$ transition, for example, is polarized along the C=C double bond. The magnitude of the transition is characterized by its absolute-value squared, which is called the dipole strength, D_{GE} :

$$D_{GE} = |\mu_{GE}|^2$$

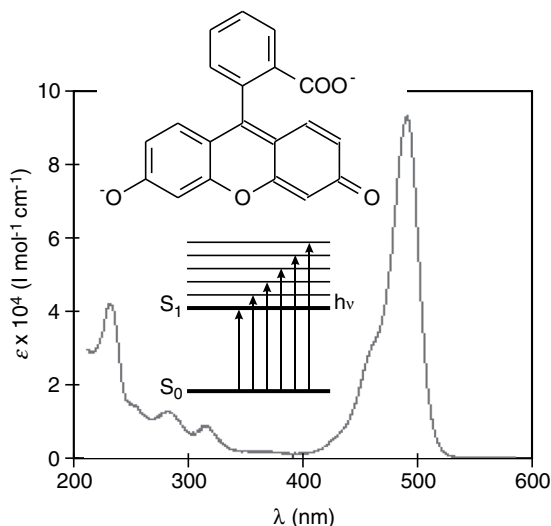


Figure 1.3 Molecular structure and absorption spectrum of the dianion fluorescein in ethanol, pH 9.0. The inset also shows the electronic ground and first excited singlet state level and possible absorptive transitions involving different vibronic states.

A peculiarity of the absorption spectra of organic dyes as opposed to atomic spectra is the width of the absorption band, which usually covers several tens of nanometers. This is easy to understand recalling that a typical dye molecule is composed of several tens of atoms, giving rise to manifold vibrations of the skeleton. These vibrations together with their overtones densely cover the spectrum between a few wave numbers and 3000 cm^{-1} . Furthermore, most of these vibrations are coupled to the electronic transitions through the change in electron densities over the bonds constituting the conjugated chain. That is, after electronic excitation the electron density changes, which is associated with a change in bond length. Quantum mechanically this means that transitions have occurred from the electronic and vibrational ground state S_0 of the molecule to an electronically and vibrationally excited state S_1 . This results in broad absorption spectra like that shown for the fluorescein dianion in Figure 1.3 and depends on how many of the vibrational sublevels spaced at $h\nu (n + \frac{1}{2})$, with $n = 0, 1, 2, 3, \dots$, are reached and what the transitions moments of these sublevels are.

1.3

Lambert–Beer Law and Absorption Spectroscopy

Lambert–Beer Law is a mathematical means of expressing how light is absorbed by matter (liquid solution, solid, or gas). The law states that the amount of light emerging from a sample is diminished by three physical phenomena: (i) the amount of absorbing material (concentration c), (ii) the optical path length l , that is, the

distance the light must travel through the sample, and (iii) the probability that the photon of that particular energy will be absorbed by the sample (the extinction coefficient ϵ of the substance). Considering a sample of an absorbing substance placed between two parallel windows that transmit the light and supposing that the light of intensity I_0 is incident from the left, propagates along the x direction, then the intensity I decreases smoothly from left to right and exits with an intensity I_t . If the sample is homogeneous, the fractional decrease in light intensity is the same across a small interval dx , regardless of the value of x . As the fractional decrease for a solution depends linearly on the concentration of the absorbing molecule, the fractional change in light intensity dI/I can be written as:

$$-\frac{dI}{I} = \alpha c dx$$

where

α is a constant of proportionality.

Because neither α nor c depends on x , integration between limits I_0 at $x = 0$ and I_t at $x = l$, provides

$$\ln \frac{I_0}{I_t} = \alpha c l \quad \text{or} \quad I_t = I_0 e^{-\alpha c l}$$

For measurements made with cuvettes of different path lengths, the transmitted intensity, I_t , decreases exponentially with increasing path length. Alternatively, the transmitted intensity decreases exponentially with increasing concentration of an absorbing solute. The absorbance or optical density, A , is defined as base 10 rather than natural logarithms,

$$A = \log \frac{I_0}{I_t} = \epsilon c d$$

where

$\epsilon = \alpha/2.303$ is the molar extinction coefficient (or molar absorptivity) with units $M^{-1} \text{ cm}^{-1}$, when the concentration, c , and the path length, d , are given in molarity, M , and cm , respectively.

The Lambert–Beer Law shows that the absorbance is proportional to the concentration of the solute and path length with ϵ as the proportionality constant. The relationship between absorbance and transmission, $T = I_t/I_0$ is given by

$$A = -\log T$$

Because the absorption intensity depends strongly on wavelength, the wavelength at which the measurement was performed always has to be specified. The wavelength dependence of ϵ or of A is known as the absorption spectrum of the compound (Figure 1.3).

When measuring absorption spectra, several error sources have to be considered. Firstly, it should be known that a small but significant portion of light is lost by

reflection at the cuvette windows. Corrections for this effect, as well as for absorption by the solvent (in addition to absorption by the solute), are usually made by performing a parallel measurement (double-beam method) using a cuvette containing only solvent. The transmitted intensity of this second measurement is then used as I_0 in the Lambert–Beer expression. Secondly, deviations can arise from inhomogeneous samples, light scattering by the sample, dimerization or aggregation at higher concentrations, or changes in equilibrium. The most common consequence is that the measured absorbance does not increase linearly with increasing concentration or path length. Finally, excitation and subsequent fluorescence emission can significantly deteriorate the shape of the absorption spectrum of solutes with high fluorescence quantum yield at higher concentrations.

One of the most widely used applications of absorption spectroscopy is the determination of the concentration of substances in solution. Through the knowledge of the extinction coefficient, ϵ , absolute concentrations can be easily calculated using the Lambert–Beer relationship ($c = A/\epsilon d$). However, it has to be pointed out here that the extinction coefficients of common fluorophores, which are generally in the range of 10^4 – 10^5 l mol⁻¹ cm⁻¹, do not represent inherently constant parameters. Conjugation of fluorophores to or interactions with other molecules can change the extinction coefficient by influencing, for example, the planarity of the conjugated π -electron system, thereby affecting the transitions strength. Likewise, the extinction coefficient can vary with the solvent. Furthermore, the dimerization of fluorophores and formation of higher order aggregates in solution and the solid state can induce dramatic color changes, that is, changes of the extinction coefficients.

1.4

Fluorophore Dimerization and Isosbestic Points

Deviations of Lambert–Beer Law behavior for the solution spectra of organic dyes is generally attributed to aggregation of dye molecules. Aggregation of dye molecules, as measured by deviations from ideality, has been found in several classes of solvents for concentration ranges typically in the order of from 10^{-6} to 10^{-4} M. Molecular aggregates are macroscopic clusters of molecules with sizes intermediate between crystals and isolated molecules. In the mid-1930s Scheibe [4] and, independently Jelley [5] discovered that when increasing the concentration of the dye pseudoisocyanine (PIC) in water, a narrow absorption band arises, red shifted to the monomer band. The narrow absorption band was ascribed to the optical excitation of the aggregates formed. To form the simplest aggregate, a dimer, the dye–dye interaction must be strong enough to overcome any other forces which would favor solvation of the monomer.

Usually, dye aggregates are classified on the basis of the observed spectral shift of the absorption maximum relative to the respective absorption maximum of the monomer. For the majority of possible dimer geometries, two absorption bands arise, one at higher energy relative to the monomer band, termed H-type aggregates (absorption band shifted hypsochromic), and at lower energy relative to the monomer

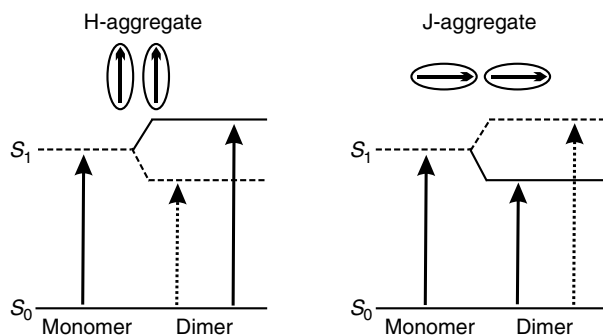


Figure 1.4 Simplified schematic of exciton theory to explain the different absorption and fluorescence behaviors of H- and J-aggregates.

band, termed J-type or Scheibe-type aggregates (absorption band shifted bathochromic) [6–12]. J-type aggregates exhibit a bent or head-to-tail structure and usually show fluorescence with an intensity that fairly often surpasses that of the monomeric dyes. In contrast, it is known that the fluorescence of face-to-face-stacked H-type dimer aggregates (sandwich-type dimers) is strongly quenched. In fact, with the exception of a few examples [13], the non-emissive character of the excited state has become commonly accepted as a general feature of H-aggregates.

According to exciton theory of Kasha *et al.* [7], in J-aggregates, only transitions to the low energy states of the exciton band are allowed and, as a consequence, J-aggregates are characterized by a high fluorescence quantum yield. In contrast, H-aggregates are characterized by a large Stokes-shifted fluorescence that has a low quantum yield (Figure 1.4). After exciting the H-exciton band, a rapid downwards energy relaxation occurs to the lower exciton states that exhibit vanishingly small transition dipole moments. Therefore, their fluorescence is suppressed and a low fluorescence yield characterizes the H-aggregates. These two different types of aggregates, the J- and H-aggregates, are distinguished by the different angle α between the molecular transition dipole moments and the long aggregate axis.

When $\alpha > 54.7^\circ$, H-aggregates are formed and when $\alpha < 54.7^\circ$, J-aggregates are formed. In general, when there is interaction between two or more molecules in the unit cell of the aggregate, two or more excitonic transitions with high transition moment are observed and the original absorption band is split into two or more components. This splitting depends on the distance between the molecules, the angle of their transition dipole moments with the aggregate axis, the angle of the transition dipole moments between neighboring molecules and the number of interacting molecules. The appearance of isosbestic points in the absorption spectrum with increasing dye concentration provides good evidence for an equilibrium between monomeric and dimeric species and enables the association constant to be calculated, in addition to the spectra of the pure monomer and dimer.

A wavelength at which two or more components have the same extinction coefficient is known as an isosbestic wavelength or isosbestic point. When only two absorbing compounds are present in solution, one or more isosbestic points are

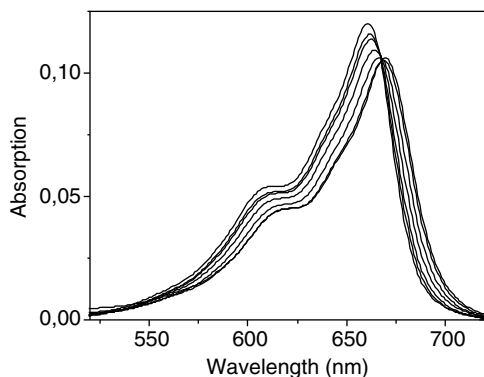
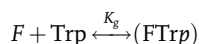


Figure 1.5 Absorption spectrum of the fluorophore MR121 measured in PBS (phosphate-buffered saline), pH 7.4, with increasing tryptophan concentration

(0–50 mM). The appearance of isosbestic points at 531 and 667 nm indicates the formation of 1 : 1 complexes for tryptophan concentrations less than 20 mM [12].

frequently encountered in the absorption spectrum. In multicomponent solutions isosbestic points almost never occur because the probability that three or more compounds have identical molar absorbances at any wavelength is negligibly small. Owing to this low probability, the occurrence of two or more isosbestic points demonstrates the presence of two and only two components absorbing in the observed spectral region. However, this rule does not apply if two chemically distinct components have identical absorption spectra (e.g., adenosine triphosphate, ATP, and adenosine diphosphate, ADP). In this case the entire spectrum represents a set of isosbestic points for these two components alone. Isosbestic points are especially useful for the study of equilibrium reactions involving absorbing reactants and products. Here, the presence of isosbestic points can be used as evidence that there are no intermediate species of significant concentration between the reactants and products. For example, besides dimer formation, several fluorophores (e.g., rhodamine and oxazine dyes) show isosbestic points in the absorption spectra upon addition of the amino acid tryptophan or the DNA nucleotide guanosine monophosphate, dGMP, in aqueous solvents (Figure 1.5) [14–16]. Usually, the extinction of the fluorophores decreases slightly upon addition of dGMP or tryptophan and the absorption maxima shift bathochromically (that is, towards longer wavelengths) by up to ~ 10 nm. The appearance of isosbestic points suggests that an equilibrium is established between two species and reflect the formation of 1 : 1 complexes between free fluorophores (F) and tryptophan (Trp). Both types absorb in the same region. At higher tryptophan concentrations (above 20 mM) slight deviations can be observed indicating a low probability of the formation of higher aggregated complexes.

The equilibrium state between free fluorophores and fluorophore/Trp-complexes can be described by [17]



where the equilibrium constant, defined as

$$K_g = \frac{[F\text{Trp}]}{[F][\text{Trp}]}$$

can be calculated using the relationship given by Ketelaar *et al.* [18]

$$\frac{1}{\varepsilon - \varepsilon_F} = \frac{1}{K_g(\varepsilon_{F\text{Trp}} - \varepsilon_F)} \frac{1}{[\text{Trp}]} + \frac{1}{\varepsilon_{F\text{Trp}} - \varepsilon_F}$$

Here ε , ε_F , and $\varepsilon_{F\text{Trp}}$ are the apparent absorption coefficient, the absorption coefficient of the fluorophores and the complex under study, respectively. By the plotting of $(\varepsilon - \varepsilon_F)^{-1}$ versus $[\text{Trp}]^{-1}$ the equilibrium constant, K_g , can be calculated from the intercept and the slope of the resulting straight line. For the addressed interactions between rhodamine and oxazine dyes with tryptophan or dGMP, equilibrium constants in the range of 50–200 M⁻¹ have been measured [14–16, 19, 20].

1.5

Franck–Condon Principle

For relatively large fluorophores containing more than 30 atoms, such as the organic dye molecules generally used in fluorescence spectroscopy and imaging, many normal vibrations of differing frequencies are coupled to the electronic transition. In addition, collisions and electrostatic interactions with surrounding solvent molecules broaden the lines of vibrational transitions. Furthermore, every vibrational sublevel of every electronic state has superimposed on it a ladder of rotational states that are significantly broadened because of frequent collisions with solvent molecules, which seriously hinder rotation. This results in a quasicontinuum of states superimposed on every electronic level. The population of the levels in contact with the thermalized solvent molecules is determined by the Boltzmann distribution. In the quantum mechanical picture, vibrational levels and wavefunctions are those of quantum harmonic oscillators and rigid rotors (with some corrections for rotation–vibration coupling and centrifugal distortion) (Figure 1.6a).

The more realistic anharmonic potential (e.g., the Morse potential) describing the vibrational dynamics of a molecule is, in general, different for each electronic state. Excitation of a bound electron from the HOMO to the LUMO increases the spatial extent of the electron distribution, making the total electron density more diffuse, and often more polarizable. Thus, one finds in general that the bond length between two atoms in a diatomic molecule is larger and the bond strength is weaker in electronically excited states. On the other hand, a slightly weaker bond means that the force constant for vibrations will be lower, and the relationship between the force constant and the second derivative of the potential V ($k = d^2V/dx^2$) indicates that the weaker force constant in the excited state implies not only a lower vibrational frequency but simultaneously a broader spatial extent for the energy potential curve.

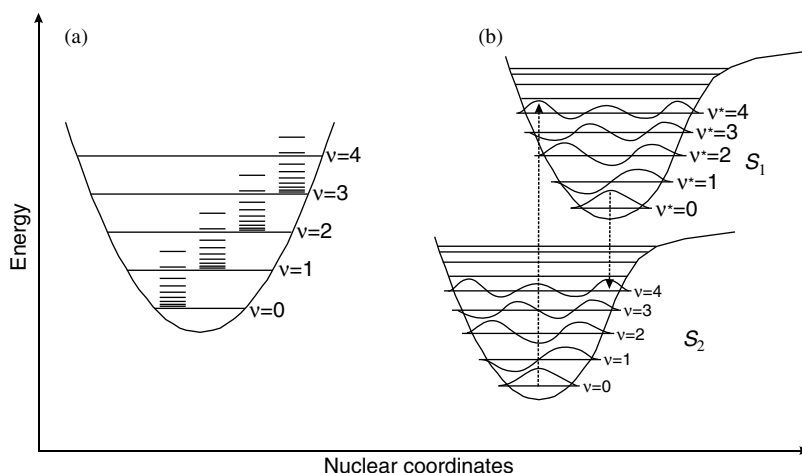


Figure 1.6 (a) Idealized potential energy curve for a diatomic molecule. In general, polyatomic molecules will have $3N - 6$ vibrational modes ($\nu_1, \nu_2, \nu_3, \dots$), where N is the number of atoms, and will be asymmetric rotors with three different inertial axes. For each of the $3N - 6$ normal vibrations, a potential well exists with a rotational energy ladder. (b) Morse potentials for a molecule in the singlet ground state S_0 and first excited singlet state S_1 to demonstrate the

Franck–Condon principle. As electronic transitions are very fast compared with nuclear motions, vibrational levels are favored when they correspond to a minimal change in the nuclear coordinates. The potential wells shown favor transitions between $\nu = 0$ and $\nu = 4$. In the simplest case of a diatomic molecule, the nuclear coordinate axis refers to the internuclear distance.

Figure 1.6b illustrates the principle for vibrational transitions in a molecule with Morse-like potential energy functions in both the ground and excited electronic states. At room temperature the molecule generally starts from the $\nu = 0$ vibrational level of the ground electronic state as the vibrational energy will normally be $1000\text{--}3000\text{ cm}^{-1}$, many times the thermal energy kT , which is about 200 cm^{-1} at room temperature. In contrast, pure rotational transitions require energies in the range of 100 cm^{-1} , that is, higher excited rotational levels are occupied at room temperature. Upon absorption of a photon of the necessary energy, the molecule makes a so-called vertical transition to the excited electronic state. The occurrence of vertical transitions on the potential energy curve is explained by the Franck–Condon principle and the Born–Oppenheimer approximation. The Born–Oppenheimer approximation is based on the fact that the proton or neutron mass is roughly 1870 times that of an electron and that electrons move much faster than nuclei. Thus, electronic motions when viewed from the perspective of the nuclear coordinates occur as if the nuclei were fixed in place. Applying the Born–Oppenheimer approximation to transitions between electronic energy levels, led Franck and Condon to formulate the Franck–Condon principle. Classically, the Franck–Condon principle is the approximation that an electronic transition is most likely to occur without changes to the position of the nuclei in the molecular entity and its

environment. The quantum mechanical formulation of this principle is that the intensity of a vibrational transition is proportional to the square of the overlap integral between the vibrational wavefunctions of the two states that are involved in the transitions [21–24]. In other words, electronic transitions are essentially instantaneous compared with the time scale of nuclear motions. Therefore, if the molecule is to move to a new vibrational level during the electronic transition, this new vibrational level must be instantaneously compatible with the nuclear positions and momenta of the vibrational level of the molecule in the originating electronic state. In the semiclassical picture of vibrations of a simple harmonic oscillator, the necessary conditions can occur at the turning points, where the momentum is zero.

Because the electronic configuration of a molecule changes upon excitation (Figure 1.6b) the nuclei must move to reorganize to the new electronic configuration, which instantaneously sets up a molecular vibration. This is the reason why electronic transitions cannot occur without vibrational dynamics. After excitation has led to a transition to a nonequilibrium state (Franck–Condon state), the approach to thermal equilibrium is very fast in liquid solutions at room temperature, because a large molecule such as a fluorophore experiences at least 10^{12} collisions per second with solvent molecules, so that equilibrium is reached in a time of the order of one picosecond. Thus, the absorption is practically continuous all across the absorption band. In the electronic excited state, molecules quickly relax to the lowest vibrational level (Kasha's rule). Dependent on their fluorescence quantum yield they can then decay to the electronic ground state via photon emission. The Franck–Condon principle is applied equally to absorption and to fluorescence. Kasha's rule states that emission will always occur from the lowest lying electronically excited singlet state $S_{1,v=0}$. The applicability of the Franck–Condon principle in both absorption and emission, along with Kasha's rule, leads to the mirror symmetry of the absorption and the fluorescence spectrum of typical organic dye molecules (Figure 1.7a). Owing to the loss of vibrational excitation energy during the excitation/emission cycle fluorescence emission always occurs at lower energy, that is, spectrally red-shifted (the so-called Stokes shift). The Stokes shift, named after the Irish physicist George

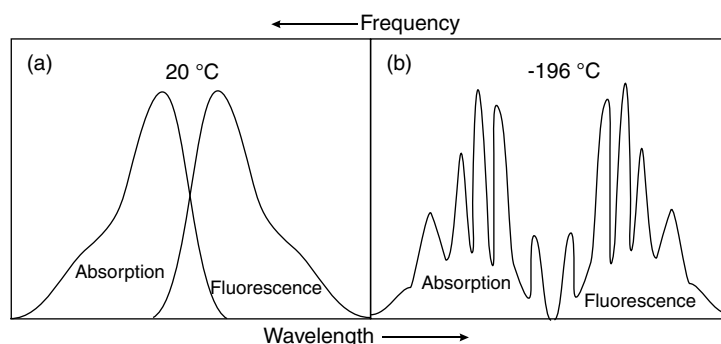


Figure 1.7 (a) Absorption and fluorescence spectrum of a typical organic dye molecule in solution (a) at room temperature (20 °C) and (b) at $-196\text{ }^{\circ}\text{C}$.

G. Stokes, represents the basis for the high sensitivity of fluorescence spectroscopy compared with other spectroscopic methods because elastic scattering of the excitation light (Rayleigh-scattering) can be efficiently suppressed using appropriate filtering.

1.6

Temperature Effects on Absorption and Emission Spectra

On increasing the temperature, higher vibrational levels of the ground state are populated according to the Boltzmann-distribution and more and more transitions occur from these levels to higher vibrational levels of the first excited electronic state. As a result, the absorption spectrum becomes broader and the superposition of the different levels blurs most of the vibrational fine structure of the band. On the other hand, at lower temperatures, the spectral widths are usually reduced and the spectra exhibit enhanced vibrational information (Figure 1.7b). Therefore, dye solutions that form a clear organic glass when cooled down to 77 K show spectra comparable to theoretical calculations because of their well-resolved vibrational structure. Further cooling below the glass point, when the free movement of solvent molecules or parts thereof is inhibited, usually brings about no further sharpening of the spectral features. However, using a matrix of *n*-paraffins at temperatures below 20 K, very sharp, line-like spectra with a width of about only 1 cm^{-1} often appear, instead of the more diffuse-like band spectra of dye molecules. This so-called “Shpol’ski effect” [25] results because there are only a few different possibilities for solvation of the molecule in that specific matrix, and each of the different sites causes a series of spectral lines in absorption as well as in emission.

Generally speaking, the zero-phonon line and the phonon sideband jointly constitute the line shape of individual light absorbing and emitting molecules embedded into a transparent solid matrix. A phonon is a quantized mode of vibration occurring in a rigid crystal lattice, such as the atomic lattice of a solid. When the host matrix contains many chromophores, each will contribute a zero-phonon line and a phonon sideband to the absorption and emission spectra. The spectra originating from a collection of identical fluorophores in a matrix is said to be inhomogeneously broadened, because each fluorophore is surrounded by a somewhat different matrix environment that modifies the energy required for an electronic transition. In an inhomogeneous distribution of fluorophores, individual zero-phonon line and phonon sideband positions are therefore shifted and overlapping. The zero-phonon line is determined by the intrinsic difference in energy levels between the ground and excited states (corresponding to the transition between $S_{0,v=0}$ and $S_{1,v=0}$) and by the local environment. The phonon sideband is shifted to higher frequency in absorption and to lower frequency in fluorescence. The distribution of intensity between the zero-phonon line and the phonon sideband is strongly dependent on temperature. At room temperature the energy is high enough to excite many phonons and the probability of zero-phonon transitions is negligible. At lower temperatures, in particular at liquid helium temperatures, however, being dependent on the strength

of coupling between the chromophore and the host lattice, the zero-phonon line of an individual molecule can become extremely narrow. On the other hand, the centers of frequencies of different molecules are still spread over a broad inhomogeneous band.

Inhomogeneous broadening results from defects in the solid matrix that randomly shift the lines of each individual molecule. Therefore, for each particular laser frequency, resonance is achieved for only a small fraction of molecules in the sample [26, 27]. In single-molecule spectroscopy (SMS) in solids at low temperature exactly this effect is used to isolate single fluorophores by their specific optical transition frequency (the zero-phonon line), which can be addressed selectively using a narrow line width laser source. The extreme sensitivity to their local environment of the sharp excitation lines of fluorophores at cryogenic temperatures enables the refined investigation of the coupling of chromophores with their surrounding matrix [27–30]. Usually, small changes in the absolute position of the purely electronic zero-phonon line absorption of single molecules were recorded by scanning the frequency of a narrow bandwidth laser used for excitation, and collecting the integral Stokes shifted fluorescence signal. The first optical detection of single molecules by Moerner and Kador in 1989 was performed in a solid at low temperature using a sensitive doubly modulated absorption method [28]. In 1990, Orrit and Bernard showed that fluorescence excitation spectra enhance the signal-to-noise ratio of single molecule lines dramatically [29]. The strong signals and the possibility to study an individual molecule for extended periods of time which is, for example, impossible in liquid solution because of rapid diffusion, paved the way for many other experiments, such as the measurement of external field effects by Wild *et al.* in 1992 [30].

The shape of the zero-phonon line is Lorentzian with a width determined by the excited-state lifetime T_{10} , according to the Heisenberg uncertainty principle. Without the influence of the lattice, the natural line width (full width at half maximum) of the fluorophore is $\gamma_0 = 1/T_{10}$. The lattice reduces the lifetime of the excited state by introducing radiationless decay mechanisms. At absolute zero, the lifetime of the excited state influenced by the lattice is T_1 . Above absolute zero, thermal motions will introduce random perturbations to the fluorophores local environment. These perturbations shift the energy of the electronic transition, introducing a temperature dependent broadening of the line width. The measured width of a single fluorophore's zero-phonon line, the homogeneous line width, is then $\gamma_h(T) \geq 1/T_1$.

Considering an ensemble of molecules absorbing with very narrow homogeneous lines (ideally at zero temperature), that is, irradiated with a monochromatic excitation source, only the resonant molecules will absorb light significantly. Upon excitation, the molecule might undergo a number of possible photophysical and photochemical processes, such as intersystem crossing into long-lived triplet states that exhibit different absorption characteristics (generally lower) at the excitation wavelength. Thus, the sample will absorb less at the frequency of illumination during the lifetime of the triplet state. If an absorption spectrum of the sample is measured it will show a transient spectral hole at the laser frequency used to excite the sample (Figure 1.8). Some of the product states may have very long lifetimes, in particular if the molecule undergoes a chemical reaction. In that case, the spectral hole is

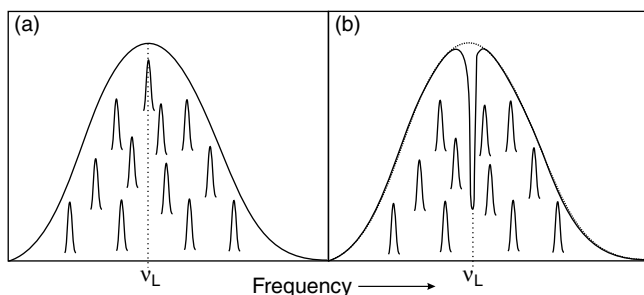


Figure 1.8 Hole-burning represents the modification of the optical properties of a material upon irradiation with light. Different environments in a disordered matrix shift the zero-phonon lines of single molecules at random. The resulting ensemble spectrum is inhomogeneously broadened as a result of the superposition of many narrow lines of individual

molecules. The figure shows the inhomogeneous absorption spectrum of an ensemble of molecules before (a) and after (b) illumination at a specific laser frequency ν_L . The sharp spectral hole appears because the narrow lines of the excited molecule are shifted to new frequencies.

permanent. In photophysical processes, the conformation of neighboring atoms or groups of atoms can be modified by illumination, leading to a shift of the absorption line, much larger than the homogeneous width, but usually smaller than the inhomogeneous bandwidth. The resulting antihole is much broader than the hole and can only be seen after very deep and broad holes have been burned.

1.7

Fluorescence and Competing Processes

The electronic states of most organic molecules can be divided into singlet states and triplet states, where all electrons in the molecule are spin paired or one set of electron spins is unpaired, respectively. Upon excitation of fluorophores with light of suitable wavelength (which can be considered as an instantaneous process occurring at time scales of $\leq 10^{-15}$ s) the fluorophore generally resides in one of the many vibrational levels of an excited singlet state (see Jablonski diagram shown in Figure 1.9). The probability of finding the molecule in one of the possible excited singlet states, S_n , depends on the transition probabilities and the excitation wavelength. In other words, the occupation of singlet states is controlled by the interaction of the electron involved in the transition with the electric field of the excitation light. Upon excitation to higher excited singlet states, molecules relax through internal conversion to higher vibrational levels of the first excited singlet state, S_1 , within 10^{-11} – 10^{-14} s. Molecules residing in higher vibrational levels will quickly (10^{-10} – 10^{-12} s) fall to the lowest vibrational level of this state via vibrational relaxation by losing energy to other molecules through collisions. From the lowest lying vibrational level of the first excited singlet state, the molecule can lose energy via radiationless internal conversion followed by vibrational relaxation.

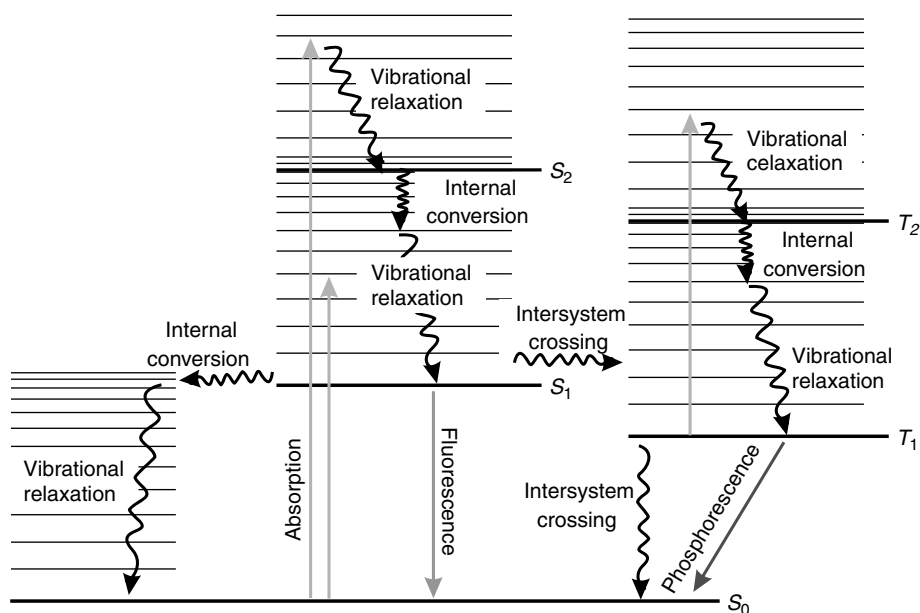


Figure 1.9 Jablonski diagram describing the electronic levels of common organic molecules and possible transitions between different singlet and triplet states.

Alternatively, the molecule might be excited into higher singlet states by absorption of a second photon. Singlet–singlet absorption ($S_1 \rightarrow S_n$) and subsequent ionization of the molecule represents a possible photobleaching pathway. The efficiency of the process depends on the absorption spectra transition strengths of the higher excited states involved, that is, whether absorption into higher excited singlet states is in resonance with the excitation light.

Depending on the molecular structure, radiative depopulation of S_1 might occur by spontaneous emission of a fluorescence photon. According to the Franck–Condon principle, the vertical transition to higher excited vibrational levels of S_0 is followed by vibrational relaxation until thermal equilibrium, according to the Boltzmann distribution, is reached. Both vibrational relaxation and internal conversion cause heating of the solvent, which thus offers an elegant method to determine the fluorescence quantum yield of fluorophores via measurement of the solvent temperature of related parameters, for example, the refractive index. Generally speaking, loose and floppy molecules exhibiting several rotational and vibrational degrees of freedom will seriously exhibit lower fluorescence intensity.

The spin of an excited electron can also be reversed by intersystem crossing, usually leaving the molecule in the first excited triplet state, T_1 . In most organic dyes intersystem crossing is fairly inefficient as a spin forbidden process, even though the triplet state is of lower electronic energy than the excited singlet state. The probability

of intersystem crossing increases if the vibrational levels of the two states overlap. For example, the lowest singlet vibrational level can overlap one of the higher vibrational levels of the triplet state. Overall, the intersystem crossing efficiency strongly depends on the nature of the fluorophore and the transition probabilities and is generally not predictable. However, it is known [31] that the presence of heavy atoms can substantially increase the intersystem crossing rate constant.

A molecule in a high vibrational level of the triplet state can lose energy through collisions with solvent molecules (vibrational relaxation), leaving it at the lowest vibrational level of the triplet state. It can then again undergo intersystem crossing to a high vibrational level of the electronic singlet ground state, where it returns to the lowest vibrational level through vibrational relaxation. As in the case of singlet states, triplet states can be excited into higher excited triplet states, T_n , by absorption of a second photon. Because the triplet/singlet transition is also spin forbidden, triplet-state lifetimes can last up to 100 s, in comparison with the 10^{-7} – 10^{-9} s average lifetime of an excited singlet state. Because internal conversion and other radiationless transfers of energy compete so successfully with radiative deactivation, phosphorescence is usually seen only at low temperatures or in highly viscous media. Owing to the long lifetime of the triplet state and distinct overlap of the $T_1 \rightarrow T_n$ and the $S_0 \rightarrow S_1$ absorption spectra of most organic dye molecules, triplet states are most probably involved in photobleaching pathways [32, 33]. Photobleaching denotes the loss of fluorescence properties of a dye due to an irreversible reaction that dramatically changes the absorption and emission capabilities. Furthermore, as higher excited states are in general more reactive than their underlying ground states, they are the most likely to be involved in photobleaching pathways. Therefore, different strategies have been developed to increase the photostability of common fluorophores, especially in single-molecule experiments, with respect to the total number of photons that can be emitted and also with respect to the fluorescence emission rate itself [34].

An interesting example of a molecule with high triplet yield presents benzophenone, with a triplet yield of 100% [35]. Generally, rhodamine, oxazine, or carbocyanine derivatives are used in applications requiring high sensitivity. In air-saturated ensemble solutions, the triplet-state lifetimes, τ_T , of such dyes vary between less than 1 μ s up to several μ s, with intersystem crossing rates, k_{ISC} , ranging from 10^5 to 10^8 s^{-1} [36–40]. The efficiency of $T_1 \rightarrow T_n$ absorption strongly depends on (i) the intersystem crossing rate, k_{ISC} , that is, the probability of finding the molecules in the triplet state, (ii) the extinction coefficient $\epsilon_T(\nu)$ at the excitation wavelength, and (iii) the triplet-state lifetime, τ_T . To minimize triplet–triplet absorption, the triplet state has to be depopulated by addition of triplet quenchers such as cyclooctatetraene (COT) or molecular oxygen. Both COT and O_2 exhibit an energetically low lying triplet state that acts as an efficient acceptor for triplet–triplet energy transfer. Thus, the dye will be transferred into the singlet ground state upon contact formation with triplet quenchers. Unfortunately, to ensure high efficient triplet quenching, mM concentrations of triplet quenchers have to be added, which renders the applicability of the method more difficult. On the other hand, triplet quenchers such as anthracene, stilbene, or naphthalene derivatives (all exhibiting low lying triplet states) can be

Table 1.1 Overview of possible depopulation pathways of excited fluorophores.

Internal conversion	$S_n \rightarrow S_1, T_n \rightarrow T_1$	k_{ic}	$10^{10}\text{--}10^{14} \text{ s}^{-1}$
Internal conversion	$S_1 \rightarrow S_0$	k_{ic}	$10^6\text{--}10^7 \text{ s}^{-1}$
Vibrational relaxation	$S_{1,v=n} \rightarrow S_{1,v=0}$	k_{vr}	$10^{10}\text{--}10^{12} \text{ s}^{-1}$
Singlet–singlet absorption	$S_1 \rightarrow S_n$	k_{exc}	10^{15} s^{-1}
Fluorescence	$S_1 \rightarrow S_0$	k_f	$10^7\text{--}10^9 \text{ s}^{-1}$
Intersystem crossing	$S_1 \rightarrow T_1, S_n \rightarrow T_n, T_n \rightarrow S_n$	k_{isc}	$10^5\text{--}10^8 \text{ s}^{-1}$
Phosphorescence	$T_1 \rightarrow S_0$	k_p	$10^{-2}\text{--}10^3 \text{ s}^{-1}$
Triplet–triplet absorption	$T_1 \rightarrow T_n$	k_{exc}	10^{15} s^{-1}

coupled directly to the fluorophore via a short aliphatic chain, ensuring highly efficient intramolecular triplet–triplet energy transfer [33].

Emission of a fluorescence photon from the vibrational ground state of the first excited singlet state constitutes a spontaneous process that contains information about the environment of the fluorophore and its interactions. For example, the fluorescence emission spectrum and its maximum contain information about the polarity of the solvent, whereas the fluorescence lifetime and fluorescence quantum yield directly reflect transient quenching interactions of the fluorophore with other molecules. Table 1.1 summarizes radiative and nonradiative reaction pathways in common organic dyes and corresponding time scales, neglecting quenching by external molecules.

1.8

Stokes Shift, Solvent Relaxation, and Solvatochromism

As organic dyes consist of many atoms (typically 50–100) they thus show a manifold and complex vibrational spectrum. Accordingly, the fluorophore has a large number of energetically different transition possibilities to the vibrational ground state after excitation with light of appropriate wavelength. Owing to the solvation shell and corresponding interactions between fluorophores and solvent molecules, the resulting vibrational transitions are considerably broadened at room temperature. The complete shift of the fluorescence emission band compared with the absorption band, due to the radiationless deactivation processes, is called the *Stokes Shift*. Because the electron distribution changes upon excitation, different bonding forces and dipole moments arise. Therefore, the solvent molecules experience a new equilibrium configuration, which they adjust to within several picoseconds at room temperature. The kinetics of dielectric relaxation of solvent molecules can be followed by monitoring the time-dependent shift in the fluorescence emission spectrum with picosecond time-resolution [41–46]. If a fluorescing molecule is excited into a more polar excited state, the electronic polarization of the solvent molecules adjusts instantaneously to the new electron distribution in the molecule. In contrast, the orientational polarization of the solvent molecules does not change

instantaneously with the excitation. Therefore, the orientational polarization is not in equilibrium with the excited molecule. This means that the solvent molecules have to react by dielectric relaxation until the equilibrium configuration of the corresponding excited state is reached. The same happens upon subsequent fluorescence emission, that is, the orientational polarization remains conserved during the quasi instantaneous optical transition. Thus, the fluorescence spectrum experiences a time-dependent red-shift, which is expressed as function $C(t)$.

$$C(t) = \frac{\nu(t) - \nu(\infty)}{\nu(0) - \nu(\infty)}$$

where

$\nu(0)$, $\nu(t)$, and $\nu(\infty)$ denote the frequencies of the fluorescence emission maximum immediately after excitation, at time t , and after complete relaxation has occurred, respectively.

Typically, dielectric relaxation is completed in 10 ps. Assuming monoexponential solvent relaxation times, time-resolved fluorescence measurements at different detection wavelengths deliver the following trend: at shorter detection wavelengths ($\lambda_{\text{blue}} < \lambda$) the measured fluorescence is dominated by those molecules whose solvation shell is incompletely relaxed, whereas at longer detection wavelengths ($\lambda < \lambda_{\text{red}}$) fluorescence is controlled by molecules with completely relaxed solvation shells. Thus, the fluorescence lifetime of fluorophores always exhibits the trend $\tau_{\text{blue}} < \tau < \tau_{\text{red}}$.

Furthermore, owing to the different properties of the ground and excited states, the dipole moment changes upon excitation $\Delta\mu = \mu_e - \mu_g$, which is reflected in a shift in the absorption and emission band, which is dependent on solvent polarity (*Solvatochromism*). Therefore, charge transfer transitions, for example, in coumarin dyes, show pronounced solvatochromism effects. On the other hand, distinct shifts in absorption and emission of suitable candidates can be used advantageously for the definition of new solvent polarity parameters [47]. For a complete description of solvatochromic effects, the refractive index n and the dielectric constant ϵ_s of the solvent, in addition to the change in dipole moment of the fluorophore upon excitation, $\Delta\mu$, have to be considered. Using the Lippert equation [48, 49]

$$\nu_{\text{abs}} - \nu_{\text{em}} = \frac{2(\mu_e - \mu_g)^2}{cha^3} \left[\frac{2(\epsilon_s - 1)}{(2\epsilon_s + 1)} - \frac{2(n^2 - 1)}{(2n^2 + 1)} \right]$$

the Stokes shift ($n_{\text{abs}} - n_{\text{em}}$) can be expressed as a function of solvent properties (n , ϵ_s) and the dipole moments of the fluorophore in the ground, μ_g , and excited states, μ_e , where c is the speed of light, h is Planck's constant, and a the *Onsager radius* of the fluorophore in the respective solvent ($a \sim 60\%$ of the longitudinal axis of the fluorophore). While for coumarin dyes the Stokes shift generally increases with solvent polarity (i.e., the emission maximum shifts further bathochromically than the absorption maximum), rhodamine derivatives show negligible solvatochromism.

1.9

Fluorescence Quantum Yield and Lifetime

Both fluorescence quantum yield and lifetime are among the most important selection criteria for fluorophores in single-molecule fluorescence spectroscopy. The fluorescence quantum yield Φ_f of a fluorophore is the ratio of fluorescence photons emitted to photons absorbed. According to the following equation

$$\Phi_f = \frac{k_r}{k_r + k_{nr}}$$

the quantum yield can be described by two rate constants, the radiative rate constant, k_r , and the nonradiative rate constant, k_{nr} , comprising all possible competing deactivation pathways, such as internal conversion, intersystem crossing, or other intra- and intermolecular quenching mechanisms. Even though complete prediction of the fluorescence quantum yield of a certain fluorophore (which would theoretically allow us to design fluorophores with ideal properties) is impossible, some requirements can be formulated that advance high fluorescence quantum yields: (i) the fluorophore should exhibit a rigid structure to minimize radiationless deactivation due to rotation or vibration of fluorophore side groups, (ii) to ensure a low intersystem crossing rate constant strong spin–orbit coupling, for example, due to heavy atoms, should be avoided, and (iii) charge transfer transitions due to conjugated electron donor and acceptor groups, as for example in coumarin dyes, often show bright fluorescence. However, there are many other nonradiative processes that can compete efficiently with the emission of light and thus reduce the fluorescence quantum yield. The reduction in fluorescence efficiency depends in a complicated fashion on the molecular structure of the dye [50].

Neglecting all radiationless deactivation processes, the rate constant for radiative deactivation of the first excited singlet state, k_f , can be approximated using the *Strickler–Berg* relationship [51]:

$$k_f = 2.88 \times 10^9 \nu_0^{-2} n^2 \frac{g_g}{g_e} \int \varepsilon d\nu$$

where

n denotes the refractive index of the solvent

g_g and g_e are the degeneracy of the ground and first excited states, respectively

ε is the extinction coefficient

ν_0 is the wavenumber of the absorption maximum (the integration is executed over the entire absorption spectrum).

Thermal blooming is commonly applied to determine the absolute fluorescence quantum yield of a dye solution. A thermal blooming measurement is, in essence, a calorimetric determination of the very small temperature gradients induced by the absorption of light energy. The technique can be extremely sensitive and allows one to measure exceptionally weak absorption [52–56]. The basic idea involving power conservation is very simple. The laser power that is incident on any sample must be

equal to the sum of the power transmitted plus the power emitted as fluorescence plus the power degraded to heat. Heat generation in the region of the absorption increases the local temperature, modifies the refractive index, and induces what is, in fact, an optical lens, which is negative for most liquids. The thermal lens develops over a period of a few tenths of seconds. During that time, the laser beam is observed as an increasing (“blooming”) spot on a plane located a few meters behind the sample. Appropriate observation of the spot size with time enables the determination of the absolute fluorescence quantum yield of the sample.

The easiest way to determine the fluorescence quantum yield is the measurement of fluorescence efficiency relative to that of a standard solution. However, relative fluorescence quantum yield measurements are aggravated by many technical problems. Firstly, a fluorescence standard absorbing and emitting in the wavelength range of the dye to be investigated must be found. Unfortunately, only a few examples, such as quinine sulfate ($\Phi_f = 70\%$ in 0.1 N H_2SO_4 [57]), fluorescein ($\Phi_f = 95\%$ in 0.1 N aqueous sodium hydroxide [56]), and rhodamine 6G in addition to rhodamine 101 ($\Phi_f = 90\text{--}100\%$ [50]) at concentrations below 10^{-5} M have been characterized so far with high precision. Furthermore, as the measurements require comparison of the fluorescence efficiency of an unknown with a standard, careful attention must be given to corrections for differences in solvent, temperature, the wavelength response of monochromators and detectors, polarization effects, and so on.

The average time a molecule spends in its excited singlet state S_1 before spontaneous emission occurs is denoted as fluorescence lifetime, τ_f .

$$\tau_f = \frac{1}{k_r + k_{nr}}$$

The fluorescence lifetime of a fluorophore can be described as the decrease in the number of excited fluorophores $[F(t)^*]$ with time following optical excitation with a infinitesimally short light pulse (δ -pulse).

$$\frac{d[F(t)^*]}{dt} = -(k_r + k_{nr})[F(t)^*]$$

As the number of excited fluorophores $[F(t)^*]$ is proportional to the fluorescence intensity $I(t)$, integration between $t=0$ and t yields a single exponential function similar to a radioactive decay (Figure 1.10).

$$I(t) = I_0 \exp\left(-\frac{t}{\tau_f}\right) \quad (1.1)$$

That is, the fluorescence lifetime can be determined by measuring the time it takes the fluorescence intensity to reach $1/e$ of its original value I_0 at $t=0$ upon optical excitation with a δ -pulse. In the case of heterogeneous samples, for example, due to different interaction possibilities between the biomolecule and the attached fluorescent label, or for mixtures of fluorophores, the fluorescence decay has to be

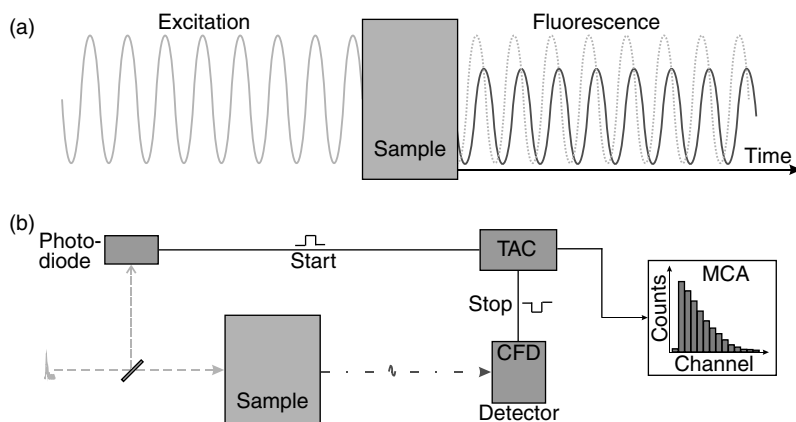


Figure 1.10 Principle of (a) phase modulation and (b) time-correlated single-photon counting (TCSPC) for the measurement of fluorescence decays.

described by applying a multiexponential model.

$$I(t) = \sum_i a_i \exp\left(-\frac{t}{\tau_{i,f}}\right)$$

$$\sum_i a_i = 1$$

Thus, time-resolved fluorescence spectroscopy enables the quantitative assignment of the relative contribution, a_i , of the i -th component of the sample with a characteristic fluorescence lifetime, $\tau_{i,f}$.

In principle, two popular methods for the determination of fluorescence lifetimes exist, the pulse or photon-counting and the phase modulation method (Figure 1.10) [58]. Instead of pulsed excitation with light pulses of duration substantially shorter than the fluorescence lifetime of the sample, the phase modulation method excites the sample with light whose intensity is modulated sinusoidally. The forced fluorescence emission of the sample directly follows the excitation modulation. Because of the finite fluorescence lifetime, emission modulation is delayed in phase by an angle relative to the excitation. In addition, fluorescence emission is demodulated due to the fact the fluorescence quantum yield of common fluorophores, Φ_f , is less than 100%. Thus, fluorescence lifetime information can be extracted from both the degree of demodulation and the phase angle. However, as phase modulation methods are inoperative for fluorescence lifetime measurements at the single-molecule level, the pulse method is mainly used. The pulse method, that is, time-correlated single-photon counting (TCSPC) [59–61], features high sensitivity and the ability to deal with low photon count rates with a time resolution down to the ps region, that is, typical parameters to be handled in single-molecule experiments.

TCSPC is based on the ability to detect and count individual photons. As it is a counting process it is inherently digital in nature. Essentially, the TCSPC technique is a start-stop or “stopwatch” technique. Usually, the excitation light pulse is split such that a photodiode is triggered at the same time that the sample is excited. It is as if a stopwatch is started at this point. When the first fluorescence photon is detected by a photomultiplier tube (PMT), microchannel plate photomultiplier (MCP), or an avalanche photodiode (APD) the stopwatch is stopped and the time lag measured is collected. This experiment is repeated several times and the start/stop time lags are plotted as a histogram to chart the fluorescence decay. The TCSPC measurement relies on the concept that the probability distribution for emission of a single photon after an excitation yields the actual intensity versus time distribution of all photons emitted as a result of the excitation. Ideally, the fluorescence intensity emitted by the sample is very low, that is, one fluorescence photon should be observed every few hundred excitation laser pulses, to prevent so-called pile-up effects. Pile-up results from the fact that a TCSPC experiment can record only one photon per excitation pulse. At high photon detection count rates, that is, when more than one fluorescence photon is produced per excitation cycle, the probability of detecting “early” emitted photons (photons with shorter arrival times) is significantly higher, thus shortening the measured fluorescence decay. To prevent pile-up effects in TCSPC measurements, the power of the excitation light should be adequately reduced.

More precisely, as the exact arrival time of a fluorescence photon at the detector is crucial for the whole TCSPC measurement, it is determined by the use of a constant fraction discriminator (CFD), which sends a precisely timed signal to *start* the charging of a linear voltage ramp in the time-to-amplitude converter (TAC). The charging linear voltage ramp of the TAC is *stopped* by the regular electronic output of the photodiode, which represents the highly stable and exact repetition rate of the optical excitation. Subsequently, a pulse is output from the TAC, the amplitude of which is proportional to the charge on the ramp, and, hence, the time between *start* and *stop*. It has to be pointed out here that the TAC is run in the inverted mode, so that each photon that is detected is counted. It takes a finite time to reset the voltage ramp and if the TAC were to be started by each laser trigger, many counts would be lost while the TAC was being reset. The pulse height is digitized by an analog-to-digital converter and a count is stored in a multi-channel analyzer (MCA) in an address corresponding to that number. These components are contained on a PC card. The MCA uses a variable number of channels (usually 512–4096 channels) that determine the time/channel. The experiment is repeated as described until the histogram of number of counts against address number corresponds to the required precision, given as a fixed number of counts at the maximum channel, the decay curve of the sample. Depending on the number of channels used, at least several thousand counts should be accumulated at the peak (Figure 1.11). The resolution of the TCSPC measurements is limited by the spread of the transit times in the detector, by the timing accuracy of the discriminator that receives the detector pulses, and by the accuracy of the time measurements. With an MCP-PMT the width of the instrument response function is of the order of 25–30 ps. The width of the time channels of the histogram can be made to be less than 1 ps.

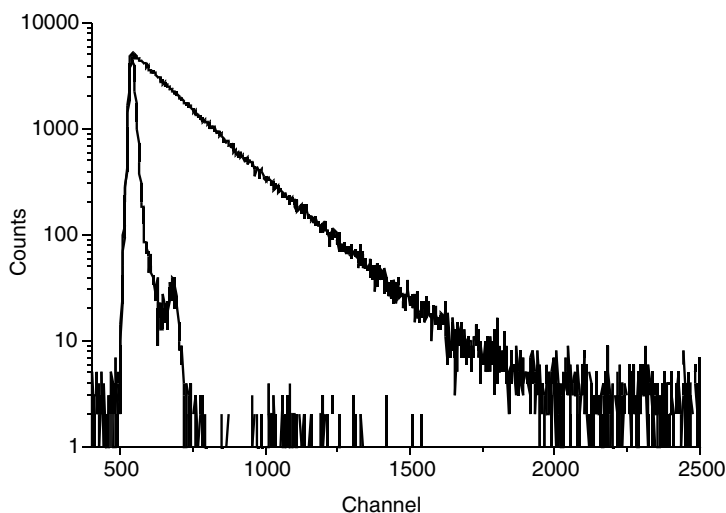


Figure 1.11 Fluorescence decay curve of a red-absorbing fluorophore and instrument response function (IRF) with a full width half maximum (FWHM) of 220 ps measured by time-correlated single-photon counting (TCSPC). For excitation, a pulsed diode laser with a repetition rate of 10 MHz and a pulse length of 200 ps (FWHM) at 635 nm is used. The

IRF is measured at the excitation wavelength using a scattering solution. The logarithmic plot of the fluorescence intensity measured at 680 nm (photon counts) versus time (4096 channels, 12 ps/channel) shows a straight line indicating monoexponential fluorescence decay behavior.

One limitation to the analysis of TCSPC measurements is the fact that, in general, the length of the laser pulse can not be neglected (Figure 1.11). Thus, the total observed fluorescence decay $R(t)$ is represented as a convolution of the instrument response function (IRF) $G(t)$ with the impulse response of the sample, which would be obtained by applying an infinitesimally small δ -pulse, $F(t)$. $G(t)$ contains all of the relevant correction factors for the detector and the complete TCSPC system:

$$R(t) = \int_0^t G(t^*) F(t-t^*) dt^* \quad (1.2)$$

The inverse process of deconvolution is mathematically difficult. Therefore, most approaches fit a sum of exponentials convoluted to an instrument response function to experimental data through an iterative convolution. In single-molecule experiments, photon statistics are generally low, which renders the application of deconvolution procedures more difficult and time-consuming. Therefore, alternative strategies appear to be more suitable. To fully maximize the information content of a TCSPC single-molecule fluorescence data set, statistical estimator techniques have been shown to give the best results when dealing with the stochastic nature of single-molecule fluorescence data. In particular, for identifying molecules based on

their fluorescence lifetime, pattern matching using the maximum likelihood estimator (MLE) technique has been shown to give the theoretically best possible identification for typical fluorophores with nanosecond fluorescence lifetimes [62–65]. In addition, the use of neuronal networks for the identification of single molecules according to their fluorescence lifetime has been shown successfully [66]. For ideal single-molecule data, it was found that the neural networks and the MLE perform almost equally well.

Most approaches to the determination of the fluorescence lifetime of single-molecule data were realized using a monoexponential MLE-algorithm [67, 68]:

$$1 + \left(e^{\frac{T}{\tau}} - 1\right)^{-1} - m \left(e^{\frac{mT}{\tau}} - 1\right)^{-1} = N^{-1} \sum_{i=1}^m i N_i$$

where

T is the width of each channel

m the number of utilized time channels

N the number of photon counts taken into account

N_i is the number of photon counts in time channel i .

Typical parameters used in single-molecule data analysis are $m = 50$ and $T = 0.2$ ns [64, 65, 69]. The left-hand side of the equation is independent of the measured experimental data and only determined by the fluorescence lifetime, τ .

However, it should be considered that in most single-molecule experiments it is not necessary to determine the fluorescence lifetime of individual unknown species precisely. Rather, the different species and their fluorescence lifetimes are known a priori and have thus to be identified and discriminated relative to each other. For the identification of different fluorescent molecules it is not necessary to collect as many photons as are necessary for an exact lifetime measurement with the TCSPC technique. Instead, a much smaller number of photons is sufficient [70–73]. The discrimination is achieved by comparing the raw data with the expected fluorescence decays measured in concentrated solutions with high precision.

1.10

Fluorescence Anisotropy

When fluorophores are excited by polarized light (e.g., by a laser), molecules whose transition dipole moments are oriented parallel to the electric field vector E will be excited preferentially. This *photo selection* similarly results in polarized fluorescence emission, which can seriously influence lifetime measurements. As transition dipole moments for absorption and emission have fixed orientations within a fluorophore, excitation of fluorophores oriented in a rigid matrix (an organic solvent at low temperature or a polymer at room temperature) with polarized light leads to significant polarization effects. For excitation with linearly polarized light the

fluorescence anisotropy, r , and polarization, P , are defined by

$$r = \frac{I_{vv} - I_{vh}}{I_{vv} + 2I_{vh}}$$

$$P = \frac{I_{vv} - I_{vh}}{I_{vv} + I_{vh}}$$

where

I_{vv} and I_{vh} are the fluorescence intensities measured upon vertical (v) excitation under parallel (vv) or perpendicular (horizontal) (vh) oriented polarizers.

If the rotational correlation time ϕ (the characteristic lifetime of rotational diffusion) is much faster than the fluorescence lifetime, τ , of the fluorophore ($\phi \ll \tau$), emission of the sample is completely depolarized ($I_{vv} = I_{vh}$ and $r = 0$). With typical fluorescence lifetimes of organic fluorophores in the nanosecond range and rotational correlation times of the order of 100 ps, fluorescence emission of organic fluorophores in low viscosity solvents (e.g., water) is depolarized. On the other hand, if ϕ is slower than τ , for example, for fluorophores conjugated to large biomolecules, measurements at lower temperatures or in solvents of high viscosity, the emission is strongly polarized. However, the maximum anisotropy, r_0 , which corresponds to the limit of a transparently frozen solvent, can only be measured infrequently because of reabsorption and the different energy transfer processes that promote depolarization. Therefore, the technique of fluorescence anisotropy can be used advantageously to study protein–protein interactions or interactions between nucleic acids and proteins in homogeneous solution.

Complete loss of anisotropy occurs when detection is performed below an angle of 54.7° , the *magic angle*, relative to the direction of polarization of the excitation light. That is, anisotropy is eliminated when the angle between the emission dipole of the fluorophore, γ , and the incident excitation light corresponds to 54.7° .

$$r = \frac{3 \cos^2 \gamma - 1}{2}$$

Time-resolved fluorescence anisotropy measurements, that is, recording of the fluorescence decay behind a polarizer in parallel and perpendicular positions relative to the linear polarization of the pulsed excitation light, enables the construction of the time-resolved fluorescence anisotropy decay, $r(t)$.

$$r(t) = r_0 e^{-\frac{t}{\phi}}$$

For spherically symmetrical molecules the anisotropy decay can be described by a monoexponential model. Multiexponential anisotropy decays imply that the molecule under investigation exhibits unsymmetrical geometry. As rotational correlation times of small organic fluorophores are of the order of 100 ps, a short excitation pulse and deconvolution methods are even more important than for time-resolved fluorescence measurements. With the aid of the rotational correlation time, measured

from time-resolved anisotropy measurements, the rotational volume of the molecule V in the solvent of viscosity η at temperature T can be determined using the gas constant, R .

$$\phi = \frac{\eta V}{RT}$$

References

- 1 Schäfer, F.P. (1973) Principles of dye laser operation, in *Topics in Applied Physics "Dye Lasers"*, vol. 1 (ed. F.P. Schäfer) Springer-Verlag Berlin, Heidelberg, New York, pp. 1–83.
- 2 Kuhn, H. (1948) *J. Chem. Phys.*, **16**, 840–841.
- 3 Kuhn, H. (1949) *J. Chem. Phys.*, **17**, 1198–1212.
- 4 Scheibe, G. (1941) *Angew. Chem.*, **49**, 567.
- 5 Jelley, E.E. (1936) *Nature*, **138**, 1009–1010.
- 6 Herz, A.H. (1977) *Adv. Colloid Interface Sci.*, **8**, 237–298.
- 7 Kasha, M., Rawls, H.R., and El-Bayoumi, M.A. (1965) *Pure Appl. Chem.*, **11**, 371–392.
- 8 Czikkely, V., Försterling, H.D., and Kuhn, H. (1970) *Chem. Phys. Lett.*, **6**, 207–210.
- 9 Scheibe, G. (1948) *Z. Elektrochem.*, **52**, 283–292.
- 10 Möbius, D. (1995) *Adv. Mater.*, **7**, 437–444.
- 11 Rabinowitch, E. and Epstein, L. (1941) *J. Am. Chem. Soc.*, **63**, 69.
- 12 Förster, T. and König, E. (1957) *Z. Elektrochem.*, **61**, 344–348.
- 13 Rösch, U., Yao, S., Wortmann, R., and Würthner, F. (2006) *Angew. Chem. Int. Ed.*, **45**, 7026–7030.
- 14 Doose, S., Neuweiler, H., and Sauer, M. (2005) *ChemPhysChem.*, **6**, 1–10.
- 15 Heinlein, T., Knemeyer, J.P., Piestert, O., and Sauer, M. (2003) *J. Phys. Chem. B*, **107**, 7957–7964.
- 16 Seidel, C.A.M., Schulz, A., and Sauer, M. (1996) *J. Phys. Chem.*, **100**, 5541–5553.
- 17 Mataga, N. and Kubota, T. (1970) Chs 3 and 7, in *Molecular Interactions and Electronic Spectra*, Marcel Dekker, New York.
- 18 Ketelaar, J.A.A., Van de Stolpe, C., Goudsmit, A., and Dzcubas, W. (1952) *Recl. Trav. Chim. Pays-Bas*, **71**, 1104.
- 19 Neuweiler, H., Schulz, A., Böhmer, A., Enderlein, J., and Sauer, M. (2003) *J. Am. Chem. Soc.*, **125**, 5324–5330.
- 20 Marmé, N., Knemeyer, J.P., Wolfrum, J., and Sauer, M. (2003) *Bioconjugate Chem.*, **14**, 1133–1139.
- 21 International Union of Pure and Applied Chemistry, (1997) *IUPAC Compendium of Chemical Terminology*, 2nd edn, Blackwell Scientific, Oxford.
- 22 Franck, J. (1926) *Trans. Faraday Soc.*, **21**, 536–542.
- 23 Condon, E. (1926) *Phys. Rev.*, **28**, 1182–1201.
- 24 Condon, E. (1928) *Phys. Rev.*, **32**, 858–872.
- 25 Shpolski, E.V. (1962) *Usp. Fiz. Nauk.*, **77**, 321.
- 26 Moerner, W.E. and Carter, T.P. (1987) *Phys. Rev. Lett.*, **59**, 2705.
- 27 Tamarat, Ph., Maali, A., Lounis, B., and Orrit, M. (2000) *J. Phys. Chem. A*, **104**, 1–16.
- 28 Moerner, W.E. and Kador, L. (1989) *Phys. Rev. Lett.*, **62**, 2535.
- 29 Orrit, M. and Bernard, J. (1990) *Phys. Rev. Lett.*, **65**, 2716.
- 30 Wild, U.P., Güttler, F., Priotta, M., and Renn, A. (1992) *Chem. Phys. Lett.*, **193**, 451.
- 31 Kasha, M. (1952) *J. Phys. Chem.*, **20**, 71.
- 32 Labhart, H. and Heinzelmann, W. (1973) *Organic Molecular Photophysics*, vol. 1 (ed. J.B. Birks) John Wiley & Sons, Ltd, Chichester, pp. 297–355.
- 33 Liphardt, B. and Lüttke, W. (1982) *Chem. Ber.*, **115**, 2997–3010.
- 34 Tsien, R.Y. and Waggoner, A. (1995) Fluorophores for confocal microscopy – photophysics and photochemistry, In: *Handbook of Biological Confocal Microscopy*, 2nd edn, (ed. J.B. Pawley) Plenum Press, New York, p. 267.

- 35 Moore, W.M.L. and Hammond, G.S. (1961) *J. Am. Chem. Soc.*, **83**, 2789–2794.
- 36 Widengren, J. and Schwille, P. (2000) *J. Phys. Chem. A*, **104**, 6416.
- 37 Asimov, M.M., Gavrilenko, V.N., and Rubinov, A.N. (1990) *J. Lumin.*, **46**, 243.
- 38 Menzel, R. and Thiel, R. (1998) *Chem. Phys. Lett.*, **291**, 237.
- 39 Menzel, R., Bornemann, R., and Thiel, E. (1999) *Phys. Chem. Chem. Phys.*, **1**, 2435.
- 40 Tinnefeld, P., Hertzen, D.P., and Sauer, M. (2001) *J. Phys. Chem. A*, **105**, 7989–8003.
- 41 Maroncelli, M. and Fleming, G.R. (1987) *J. Chem. Phys.*, **86**, 6221–6239.
- 42 Maroncelli, M., MacInnis, J., and Fleming, G.R. (1989) *Science*, **243**, 1674–1681.
- 43 Jarzeba, W., Walker, G.C., Johnson, A.E., and Barbara, P.F. (1988) *J. Phys. Chem.*, **92**, 7039–7041.
- 44 Jarzeba, W., Walker, G.C., Johnson, A.E., and Barbara, P.E. (1991) *Chem. Phys.*, **152**, 57–68.
- 45 Akeson, E., Walker, G.C., and Barbara, P.F. (1991) *J. Chem. Phys.*, **95**, 4188–4194.
- 46 Jiang, Y., McCarthy, P.K., and Blanchard, G.J. (1994) *Chem. Phys.*, **183**, 249–267.
- 47 Reichardt, C. (1979) *Angew. Chem.*, **91**, 119–131.
- 48 Lippert, E. (1957) *Z. Elektrochem.*, **61**, 962–975.
- 49 Suppan, P. (1990) *J. Photochem. Photobiol. A: Chem.*, **50**, 293–330.
- 50 Drexhage, K.H. (1973) Structure and properties of laser dyes, In: *Topics in Applied Physics “Dye Lasers”*, vol. 1 (ed. F.P. Schäfer) Springer-Verlag, Berlin, Heidelberg, New York, pp. 144–179.
- 51 Strickler, S.J. and Berg, R.A. (1962) *J. Chem. Phys.*, **37**, 814–822.
- 52 Demas, J.N. and Crosby, G.A. (1971) *J. Phys. Chem.*, **75**, 991.
- 53 Flu, C. and Whinnery, J.R. (1973) *Appl. Opt.*, **12**, 72.
- 54 Long, M.E., Swofford, R.L., and Albrecht, A.C. (1976) *Science*, **191**, 183–185.
- 55 Twarowski, A.J. and Kliger, D.S. (1977) *Chem. Phys.*, **20**, 259.
- 56 Brannon, J.H. and Magde, D. (1978) *J. Phys. Chem.*, **82**, 705–709.
- 57 Scott, T.G., Spencer, R.D., Leonard, N.J., and Weber, G.J. (1970) *J. Am. Chem. Soc.*, **92**, 687–695.
- 58 Lakowicz, J.R. (1999) *Principles of Fluorescence Spectroscopy*, 2nd edn, Plenum Press, New York.
- 59 Bollinger, T. (1961) *Rev. Sci. Instrum.*, **32**, 1044.
- 60 O'Connor, D.V. and Phillips, D. (1984) *Time-Correlated Single Photon Counting*, Academic Press, London.
- 61 Becker, W. (2005) Advanced time-correlated single photon counting techniques, In: *Springer Series in Chemical Physics*, Springer-Verlag, Berlin Heidelberg.
- 62 Enderlein, J. and Sauer, M. (2001) *J. Phys. Chem. A*, **105**, 48–53.
- 63 Maus, M., Cotlet, M., Hofkens, J., Gensch, T., De Schryver, F.C., Schaffer, J., and Seidel, C.A.M. (2001) *Anal. Chem.*, **73**, 2078.
- 64 Hertzen, D.P., Tinnefeld, P., and Sauer, M. (2000) *Appl. Phys. B*, **71**, 765.
- 65 Sauer, M., Angerer, B., Han, K.T., and Zander, C. (1999) *Phys. Chem. Chem. Phys.*, **1**, 2471.
- 66 Bowen, B.P., Scruggs, A., Enderlein, J., Sauer, M., and Woodbury, N. (2004) *J. Phys. Chem. A*, **108**, 4799–4804.
- 67 Tellinghuisen, J. and Wilkerson, C.W. Jr. (1993) *Anal. Chem.*, **65**, 1240–1246.
- 68 Enderlein, J., Goodwin, P.M., Van Orden, A., Ambrose, W.P., Erdmann, R., and Keller, R.A. (1997) *Chem. Phys. Lett.*, **270**, 464–470.
- 69 Sauer, M., Arden-Jacob, J., Drexhage, K.H., Göbel, F., Lieberwirth, U., Mühlegger, K., Müller, R., Wolfrum, J., and Zander, C. (1998) *Bioimaging*, **6**, 14–24.
- 70 Kullback, S. (1959) *Information Theory and Statistics*, John Wiley & Sons, Inc., New York.
- 71 Köllner, M. and Wolfrum, J. (1992) *Chem. Phys. Lett.*, **200**, 199–204.
- 72 Köllner, M. (1993) *Appl. Opt.*, **32**, 806–820.
- 73 Köllner, M., Fischer, A., Arden-Jacob, J., Drexhage, K.H., Seeger, S., and Wolfrum, J. (1996) *Chem. Phys. Lett.*, **250**, 355–360.